PNAS RESEARCH ARTICLE | CHEMISTRY

Design strategies for ion-sieving charge mosaic membranes toward sustainable lithium extraction

Ge Zhang[a,1], Guoliang Hu[a,1], Jinlei Li[a], Guangxia Feng[a], Yi Cui[a], Zhouyi Chen[a], Zaichun Liu[a], and Yi Cui[a,b,c,2]

Affiliations are included on p. 8.

Edited by Valeria Molinero, The University of Utah, Salt Lake City, UT; received May 9, 2025; accepted September 17, 2025

Membrane-based technologies are essential for realizing sustainable ion-sieving processes such as lithium extraction. Much effort was devoted to designing new membrane materials, whereas the effect of charge distribution has been largely overlooked. Here, we filled this knowledge gap by providing a quantitative transport model for selective ion diffusion through a charge mosaic membrane (CMM). Composed of alternating regions of Li-selective ceramic and anion-selective polymeric materials, CMMs offered the unique advantage of promoting the transport of both Li^+ and anions while blocking other cations. As a result, the membrane achieved a high Li/Mg selectivity of 62 and a high permeation rate of 59 mmol·m^{-2}·h^{-1} at a low feeding concentration of 30 mM, without any external driving force. Systematical experiments revealed the influence of brine Mg/Li ratio and membrane ceramic/polymer ratio on the overall extraction rate, which was consistent with the prediction of our transport model. The model developed in this work not only presented the design strategies of CMMs for Li extraction but also provided guidance for the development of other ion-sieving processes in general.

lithium extraction | charge mosaic membrane | selective ion transport

Significance

Membrane-based technologies received increasing attention because they could enable continuous and sustainable ion separation for energy and environmental applications. However, design principles have not been elucidated regarding charge distribution within the membranes. Here we developed a quantitative transport model for selective ion diffusion through a charge mosaic membrane (CMM), composed of alternating regions of oppositely charged materials. We showed that the concentration gradient of anion could help accelerate Li transport. As a result, the membrane achieved a high Li/Mg selectivity of 62 and a high extraction rate of 59 mmol·m^{-2}·h^{-1} at a low feeding concentration of 30 mM, without any external driving force. The model provided critical guidance for the development of CMMs for ion-sieving processes in general.

Lithium, the key ingredient of high energy density rechargeable batteries, plays a critical role in the global transition toward a sustainable future (1–4). Production of lithium is currently dominated by solar evaporation of brines and pyro/hydrometallurgical refining of hard rocks (5–7). Although mining from brine typically leaves less carbon footprint and uses less chemicals than from hard rock (8, 9), the evaporation process still poses environmental challenges as it exacerbates water loss from the arid regions surrounding the salt lakes (10, 11). Hence there is a pressing need for more sustainable lithium extraction techniques.

In recent years, membrane-based separation techniques have attracted increasing attention for ion-sieving applications because they could operate continuously and use very little chemicals (12–17). Separation of lithium ions from sodium, potassium, and magnesium ions can be quite challenging, as they have similar hydrated radii as lithium (18, 19). Modifying nanofiltration (NF) membranes with charged functional groups proved to be effective for improving mono/divalent ion selectivity based on charge exclusion and Donnan effects (19–24). However, these membranes have large pore sizes (~1 nm) and thus fall short of differentiating Li^+ from other monovalent cations, especially Na^+ and K^+ which are smaller than Li^+ when hydrated (25–27). In addition, by forcing huge amounts of water through NF membranes, most of the energy input is lost to hydrodynamic resistance during a pressure-driven filtration process.

In comparison, single ion conducting membranes have demonstrated extremely high Li ion selectivity in voltage-driven electrodialysis processes (28–30). Thanks to the small pore sizes (<0.2 nm) formed by their negatively charged lattice backbones, Na^+ and Mg^{2+} will be blocked due to either a large size after dehydration or a large dehydration energy, allowing only Li^+ to pass through (30–32). To mitigate the charge imbalance generated by transporting Li^+ through single ion conducting membranes, Hoshino and Lai and coworkers initially used water splitting reaction which caused high energy consumption (29, 30, 33–35). Fortunately, this disadvantage can be circumvented by employing reversible redox couples (H^+/H_2, Fe(III)/Fe(II) or AgCl/Ag) on the two electrodes across the membrane (36–39). Nevertheless, introducing extra redox pairs may alter the solution pH, complicate the device structure, and increase the system cost. The low ionic conductivity of the receiving solution also increases energy cost, which typically needs to be addressed by adding supplementary salts.

To avoid the necessity of redox couples and supplementary salts in ion-sieving processes, it is reasonable to introduce anion-conductive channels into a single ion conducting membrane. Charge mosaic membranes (CMM) hold great potential in that aspect, as

Author contributions: G.Z. and Y.C. designed research; G.Z., G.H., J.L., and Z.C. performed research; G.F., Y.C., and Z.L. contributed new reagents/analytic tools; G.Z. and G.H. analyzed data; and G.Z. and G.H. wrote the paper.

The authors declare no competing interest.

This article is a PNAS Direct Submission.

[1]G.Z. and G.H. contributed equally to this work.

[2]To whom correspondence may be addressed. Email: yicui@stanford.edu.

This article contains supporting information online at https://www.pnas.org/lookup/suppl/doi:10.1073/pnas.2511666122/-/DCSupplemental.

Published November 10, 2025.

they contain alternating positively and negatively charged regions that are permeable to anions and cations, respectively (20, 40). Although the concept of CMM was proposed nearly a century ago by Sollner (41–43). it received limited attention outside the area of desalination and separation of charged/noncharged solutes (40, 44–46). Very recently, several research groups began to explore the potential of CMMs for diffusion-dialytic Li extraction. Ounissi et al. observed Na^+-concentration-dependent Li^+ flux through composite membranes made from anion exchange polymers (AEP) and ceramic lithium conductor particles (47–49). Ma et al. studied the effect of porosity on the selectivity and permeability of "dual-channel membranes," which was formed by modifying the pores of a lithium conductor with AEP solutions (50). Zheng et al. were the first to deliberately cite the concept of CMMs for Li extraction in their paper, which compared the nanofiltration performance of a CMM with a dual-layer membrane made with the same materials (51). However, a quantitative and physical-based model has not been developed for diffusion-dialysis processes using CMMs.

In this work, we established a transport model to describe the Li flux through a CMM, based on systematical studies about the influence of feeding brine compositions and membrane properties. The CMM was fabricated by filling a porous lithium conductor ($Li_{1.5}Al_{0.5}Ge_{1.5}(PO_4)_3$, LAGP) pellet with an AEP, PECH-DABCO (Polyepichlorohydrin-1,4-diazabicyclo[2.2.2]octane). Such a design provided continuous pathways for both Li^+ and anions, while blocking other cations. In addition, the spatial proximity of the alternating channels ensured rapid charge neutralization after Li^+ and anions exited the membrane. Therefore, the diffusion dialysis process enabled by CMM combined multiple advantages together, including high Li flux at a low feeding concentration, competitive Li/Mg selectivity, and zero energy consumption. Moreover, we developed an equivalent circuit model for ion-sieving CMMs, which successfully captured the effects of LAGP porosity and Mg/Li ratio on Li flux observed experimentally. The theoretical framework established in this work could not only inform the optimization strategies of CMMs for Li extraction but also guide the development of other ion-sieving processes in general.

Results

Fabrication and Characterization of the Ion-Sieving Charge Mosaic Membrane. To form bicontinuous networks of both cation and anion conductive channels, a porous LAGP framework was first prepared by sintering a mixed pellet of LAGP and sacrificial polymers, then a solution of PECH-DABCO was vacuum infiltrated into the porous LAGP, as shown in Fig. 1. Polymer powder, as the binder and pore-forming agent, was ground together with commercial LAGP nanoparticles until well mixed. The mixed powder was then pressed into a green pellet and underwent a two-step sintering in air to remove the polymer and form the continuous pores. Different polymers were tested, in which microcrystalline cellulose gave rise to the best integrity and consistency among the final products (*SI Appendix*, Fig. S1). The weight ratio of cellulose to LAGP nanoparticles was adjusted to produce LAGP framework with different porosities. The nominal porosity, calculated from the mass ratio and the density of cellulose and LAGP, was always larger than the measured porosity of the postsintering pellets (*SI Appendix*, Table S1). This was likely caused by void shrinkage and crystal densification during high temperature sintering, which was also observed for pure LAGP pellets. As the mass fraction of cellulose increased from 33 to 50% in the mixture, the geometric porosity increased from 48 to 57% accordingly. In addition, the porosity measured by water filling was only half of the geometric porosity, which was based on the physical size and mass of the LAGP framework (*SI Appendix*,

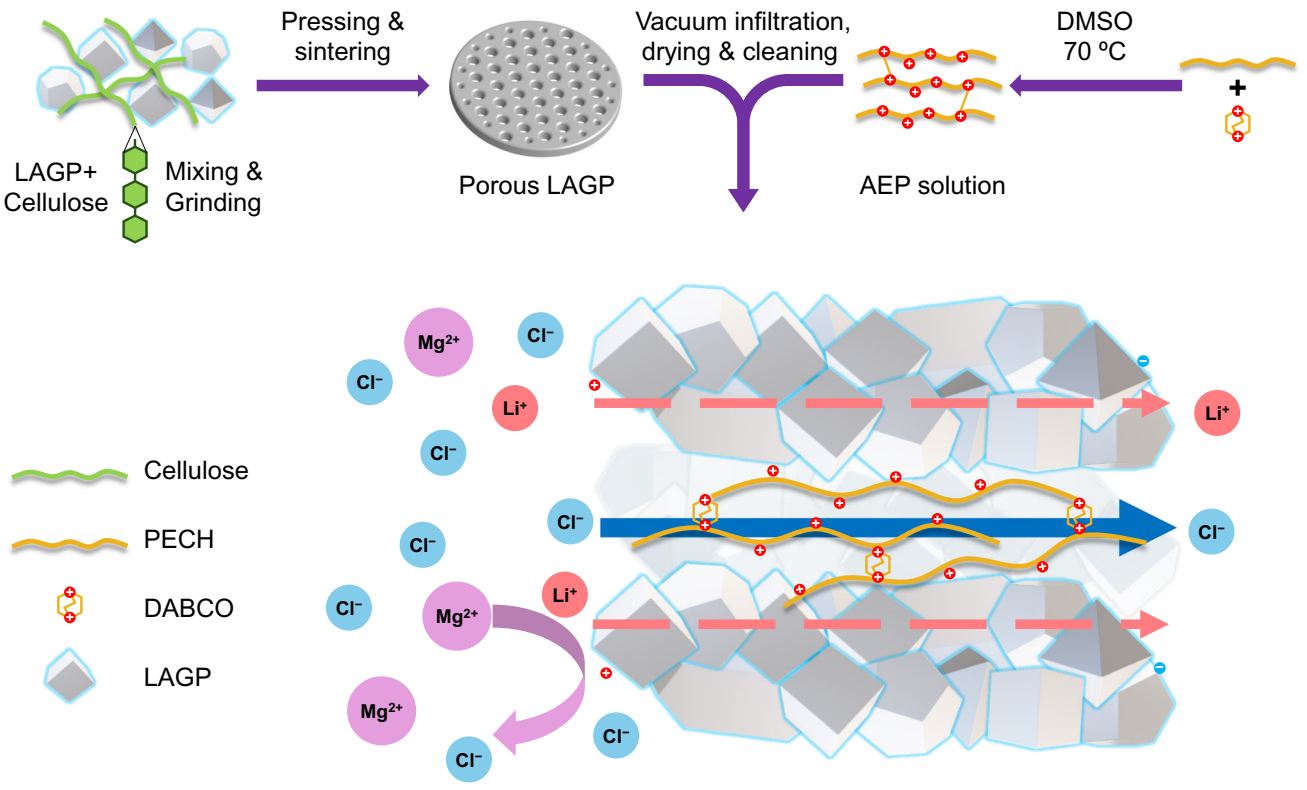

Fig. 1. Concept. Design and fabrication process of the ion-sieving charge mosaic membrane. The composite membrane was prepared by vacuum infiltrating a solution of AEP into a porous LAGP framework.

Table S1 and Note 1). Such a difference likely indicated that a large fraction of the pore volume was not accessible by simply immersing the LAGP pellets into water.

The anion exchange polymer was synthesized by the Menshutkin reaction between the alkyl chloride pendant of PECH and the tertiary diamine DABCO. After the reaction, the peaks corresponding to the stretching (ν) and bending (δ) vibrations of tertiary C–N bonds in DABCO and the stretching vibration of C–Cl bonds in PECH all showed diminished intensity (Fig. 2*A*) (52). Meanwhile, a new peak related to C–N^+ bonds appeared in both the Fourier transform infrared (FTIR) and the Raman spectra (Fig. 2 *A* and *B*), suggesting the successful formation of quaternary ammonium cations.

SEM characterization showed that the surface of the LAGP framework contained sparsely distributed pores that were a few micrometers in size (*SI Appendix*, Fig. S2). Cross-sectional SEM images revealed more interconnected pores beneath the surface that were tens of micrometers across (Fig. 2*C*), forming a sharp contrast with dense LAGP samples that had few tiny, disconnected pores (*SI Appendix*, Fig. S3). Size distribution of pores below 40 nm was calculated from nitrogen gas adsorption isotherms, which showed very similar results for LAGP with different porosities (*SI Appendix*, Fig. S4). Most of these pores were around 3 nm and likely originated from grain boundaries as they were also present in dense LAGP. The cumulative volume of mesopores was only 0.007 $cm^3 \cdot g^{-1}$, which accounted for less than 5% of the total pore volume, suggesting that macropores visible under SEM contributed the majority of total pore volume.

As mentioned above, nearly half of the pore volume inside the LAGP framework was not easily available by simple immersion, and the high viscosity of the AEP solution further aggravated the problem (*SI Appendix*, Fig. S5*A*). To facilitate the flow when incorporating the AEP solution, we employed vacuum infiltration. After infiltration, the pore wall was covered with polymeric substance visible from both the surface and the cross-section (*SI Appendix*, Fig. S5 *E*–*G*), as indicated by the yellow circles in Fig. 2 *D* and *E*. Energy-dispersive X-ray (EDS) mapping showed a similar distribution of C and Cl from AEP with Ge from LAGP on the cross section of the membrane (Fig. 2*F*), indicating a uniform coverage of AEP on the LAGP framework. C and Cl signals were more concentrated towards the surface of the LAGP membrane as shown in *SI Appendix*, Fig. S6, which was likely caused by the enrichment of the residual AEP solution during the drying process. Nonetheless, the atomic percentage remained similar across different positions on the cross section (*SI Appendix*, Fig. S7). At first glance, the infiltrated amount of AEP appeared to be too small to fill up all the pores (Fig. 2 *E* and *F*). However, the hydrophilic polymer could swell and fully occupy the pores upon immersion into water, as evidenced by the optical micrograph (*SI Appendix*, Fig. S5*B*). No water leakage was observed in an H-cell with a CMM as the barrier for over 2 d (*SI Appendix*, Fig. S8), further proving the complete occupation of pore entrance by AEP.

As reported in previous literature, the crystal structure of LAGP was vital for keeping a high Li selectivity (31, 32). X-ray diffraction (XRD) patterns (*SI Appendix*, Fig. S9) of the porous LAGP and the CMM were both identical with the standard pattern of $Li_{1.5}Al_{0.5}Ge_{1.5}(PO_4)_3$, confirming the well-preserved crystal structure after AEP infiltration. This ensured that the high selectivity Li conducting channels remained intact while the anion conducting channels were introduced. No features corresponding to polymer phases could be observed in XRD, possibly because their intensity was too low compared to the strong signal from crystalline LAGP.

LiCl/$MgCl_2$ Separation by Diffusion Dialysis Through the Ion-Sieving Charge Mosaic Membrane. Diffusion dialysis tests were carried out to evaluate the Li/Mg separation performance of the CMMs. A membrane with an area of 1 cm^2 was sandwiched between a simulated brine solution (0.5 M $MgCl_2$ + 30 mM LiCl) and deionized water. Both compartments were continuously stirred to ensure a uniform concentration. The concentration of Li^+ and Mg^{2+} ions in the receiving compartment was monitored by

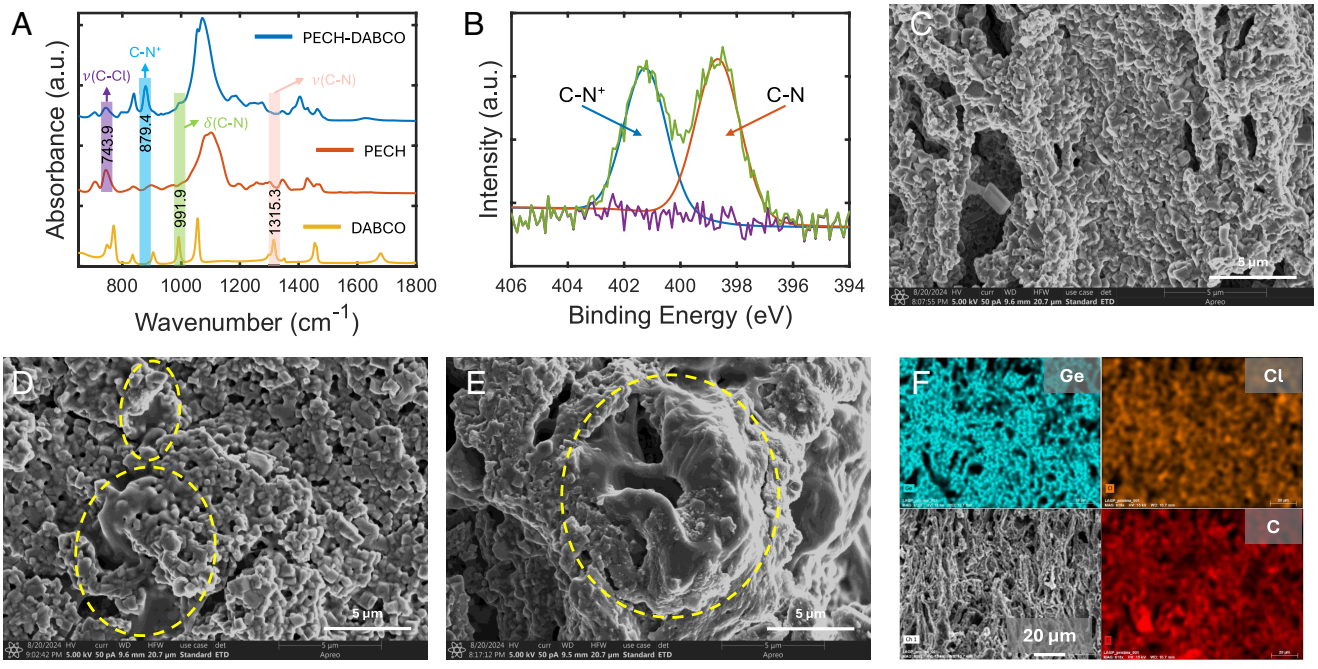

Fig. 2. Characterization of the ion-sieving charge mosaic membrane: (*A*) FTIR spectra of the synthesized PECH-DABCO polymer in comparison with the PECH polymer and DABCO crystal before crosslinking. (*B*) XPS spectra of the synthesized PECH-DABCO polymer showing the formation of quaternary ammonium groups. (*C*) Cross-sectional SEM image of the porous LAGP membrane before AEP infiltration. (*D* and *E*) SEM images of the surface (*D*) and cross section (*E*) of the CMM after AEP infiltration. The yellow dashed circles indicate the infiltrated polymer. (*F*) EDS mapping of the CMM cross section after AEP infiltration.

analyzing a small amount of liquid (50 μL) every few hours. The concentration of Li was seen to rise linearly with time in the initial 24 h, after which the rate of Li permeation slowed down slightly but remained significant even after 100 h (Fig. 3*A*). This was expected because the driving force coming from Li concentration gradient would gradually diminish as more Li^+ got extracted into the receiving chamber (*SI Appendix*, Fig. S10). In contrast, the rate of Mg leakage was very small at first but saw an increase after 24 h (Fig. 3*B*). As a result, the Li/Mg selectivity of CMMs dropped from over 300 to around 60 in 48 h (Fig. 3*C*). Nonetheless, the Mg concentration remained lower than Li even after 144 h of operation (Fig. 3 *A* and *B*), and the membrane maintained a relatively stable Li/Mg selectivity after 48 h (Fig. 3*C*). Five CMM samples were tested to ensure the reliability of the results. The difference in permeation behaviors of Li^+ and Mg^{2+} likely resulted from distinct transport pathways for the two cations. While Li^+ could travel easily through LAGP channels, Mg^{2+} was completely blocked because of its much higher dehydration energy. Mg^{2+} leakage through the AEP phase would be retarded initially due to Donnan exclusion, before a steady diffusion was established, resulting in the increase of leakage rate after 24 h observed in Fig. 3*B*.

Ideally, the CMM should be impermeable to Mg^{2+}, creating an imbalanced driving force for permeable anions (Cl^-) versus cations (Li^+). Qualitatively, this would lead to faster Li^+ permeation when Cl^- concentration was increased while Li^+ concentration was kept constant in the feeding solution. This trend was verified in experiments (Fig. 3*D*), where we varied the concentration of $MgCl_2$ from 0 to 0.5 M but fixed LiCl concentration at 30 mM. Taking the flux of Li at 48 h as an example (Fig. 3*E*), it increased quickly from 32 to 52 $mmol{\cdot}m^{-2}{\cdot}h^{-1}$ as the concentration of $MgCl_2$ was increased from 0 to 0.1 M. However, when $MgCl_2$ concentration was further increased to 0.5 M, Li flux was only slightly improved to 59 $mmol{\cdot}m^{-2}{\cdot}h^{-1}$. Li/Mg selectivity was observed to drop a little bit from 76 to 62 as $MgCl_2$ concentration varied from 0.1 M to 0.5 M (Fig. 3*F*), indicating a reliable ion-sieving performance even for high Mg/Li ratio brine (molar ratio = 16.7). At a higher feeding concentration of LiCl (150 mM), the Li extraction rate would also increase with the concentration of $MgCl_2$ (*SI Appendix*, Fig. S11 *A* and *B*). The rate was roughly proportional to the concentration of LiCl, reaching 208 $mmol{\cdot}m^{-2}{\cdot}h^{-1}$ with 150 mM of LiCl and 500 mM of $MgCl_2$ in the feeding solution. On the other hand, varying the concentration of Li did not have a significant impact on the selectivity (*SI Appendix*, Fig. S11*C*).

The composition of a CMM should also have a significant impact on its ion-sieving performance. In theory, pure LAGP (100% Li^+ selective) and pure AEP (100% Cl^- selective) membranes are both supposed to generate zero ion permeation in a diffusion dialysis setup, owing to charge neutrality requirements. Hence there naturally exists an optimal composition (LAGP:AEP volume ratio) that could maximize the Li permeability. CMMs with different LAGP porosities were tested under the same feeding and receiving conditions to study the composition effect. As expected, when the geometric porosity of LAGP was increased from 0 to 48% and 57%, the Li flux rose from nearly 0 to 25 and 59 $mmol{\cdot}m^{-2}{\cdot}h^{-1}$ (Fig. 4 *A* and *B*). This was consistent with our intuition and the previous reports from other gro (50, 53). However, further increasing the porosity of LAGP would not improve the Li permeability, as demonstrated by the lower flux (45 $mmol{\cdot}m^{-2}{\cdot}h^{-1}$) through pure AEP membranes (Fig. 4 *A* and *B*). It should be noted that these membranes (<150 μm) were much thinner than the composite CMMs (~400 μm), so their permeability was overestimated when the flux was directly compared. Unfortunately, the pure anion exchange membrane we prepared was far from ideal, which caused nonnegligible cation leakage through it even in the absence of any external voltage. This nonideality also led to decreased Li/Mg selectivity (from 327 to

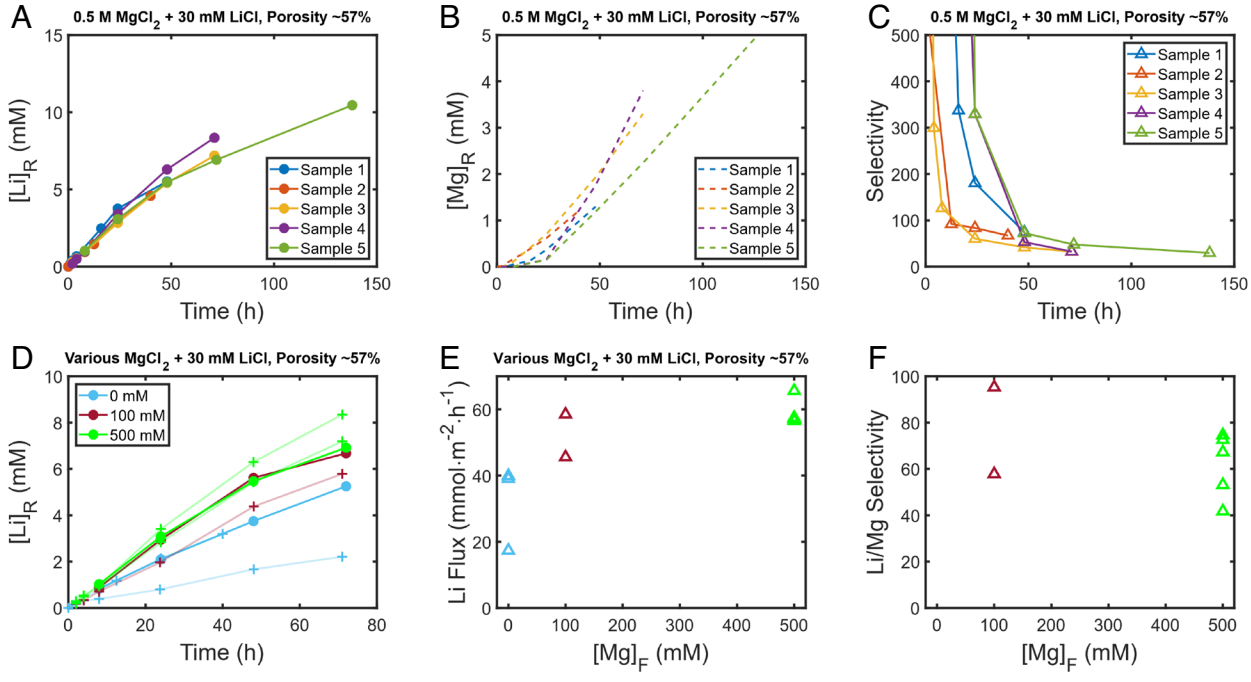

Fig. 3. LiCl/$MgCl_2$ separation performance of the ion-sieving charge mosaic membrane. (*A*) Li concentration in the receiving solution as a function of time during diffusion dialysis tests of five replicates. The feeding solution composition and the porosity of LAGP are shown in the title of the figure. (*B*) Mg concentration in the receiving solution during the same tests as in (*A*). (*C*) Evolution of Li/Mg selectivity of the five membranes during the same tests as in (*A*). (*D*) Li concentration in the receiving solution as a function of time during diffusion dialysis tests with various Mg concentrations in the feeding solution. Lines with similar colors were parallel samples. All the membranes were prepared using the same procedure. (*E*) Li flux (@48 h) as a function of Mg concentration in the feeding solution during the tests in (*D*). (*F*) Li/Mg selectivity (@48 h) as a function of Mg concentration in the feeding solution.

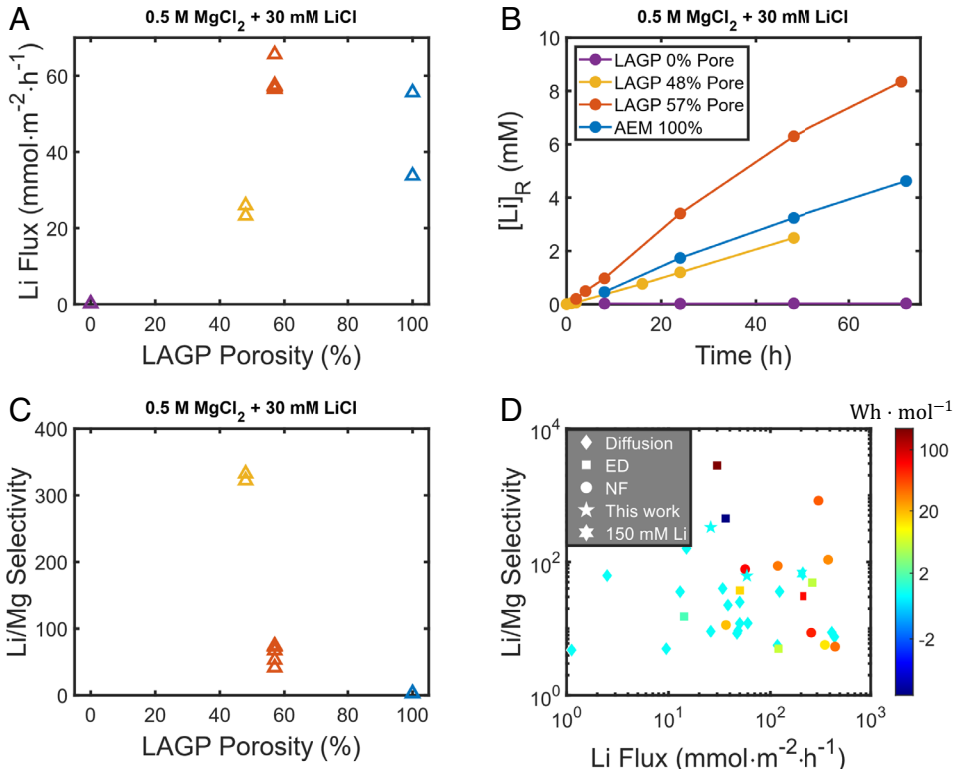

Fig. 4. Effect of LAGP porosity on the separation performance of the ion-sieving charge mosaic membrane. (*A*) Li flux (@48 h during diffusion dialysis tests) as a function of geometric porosity of LAGP. The feeding solution composition is shown in the title of the figure, 0% porosity indicates dense LAGP membrane and 100% porosity indicates pure AEP membrane. (*B*) Li concentration in the receiving solution as a function of time during diffusion dialysis tests with various LAGP porosity. (*C*) Li/Mg selectivity (@48 h during diffusion dialysis tests) as a function of geometric porosity of LAGP. The feeding solution composition is shown in the title of the figure, selectivity at 0% porosity is not measured because the membrane effectively blocked all ions. (*D*) Comparison of the Li/Mg diffusion separation performance of this work with the recent literature. The color of each data point indicates the energy consumption per mole of Li extracted.

62) with increasing volume fraction of AEP in the membrane (Fig. 4*C*). Commercial anion exchange membranes exhibited orders of magnitude lower cation leakage as well as higher Li/Mg selectivity than homemade ones (*SI Appendix*, Fig. S12), which might be attributed to their lower swelling in water and higher fixed charge density. Therefore, it is critical to improve anion selectivity of synthesized AEP in future works.

In comparison with the recent literature (39, 50, 51, 53–75), our CMMs showed competitive performance with balanced selectivity, performance, and energy consumption (Fig. 4*D*). Among the reported diffusion dialysis processes, CMMs exhibited high selectivity and high Li flux at the same time. We also noted that our performance was achieved with a lower Li concentration in the feeding brine compared to other works (*SI Appendix*, Table S2), and thus with a smaller driving force for diffusion dialysis. Although a few latest works simultaneously demonstrated higher selectivity and Li flux in electrodialysis (ED) and nanofiltration (NF) processes, they consumed much more energy to provide higher driving force as indicated by the darker color of the symbols (Fig. 4*D*, see *SI Appendix*, Table S2 for the calculation of energy consumption) (56, 62, 65). Noticeably, our previous work stood out for its negative energy cost (net energy production) with similar selectivity and permeability to the current work (39), but it had to use expensive silver electrodes and a supporting electrolyte. A comparison between the two CMMs with different LAGP:AEP ratios revealed the typical trade-off between selectivity and permeability, which again emphasized the importance of improving AEP quality in the future.

Modeling the Permeability of the Ion-Sieving Charge Mosaic Membrane. Two trends regarding the dependence of Li permeability on Cl concentration and membrane composition were observed for the CMMs in this work. Among them, the existence of an optimal composition was never discussed before. Although the dependence of Li flux on Cl concentration had been reported occasionally in the literature, no clear explanation was given (48, 53, 76). The absence of such a phenomenon in another work using membranes very similar to ours further complicated the story (50). To understand the observed performance trends and to provide guidance for future improvements, it is necessary to develop a quantitative model for the ion-sieving CMMs.

In the early literature of charge mosaic membranes, a simple yet effective equivalent circuit model was already established to describe their permeability towards solutes in single-salt solutions (77–80). However, its application towards multisalt solutions in the context of ion-sieving was not explored.

A modified equivalent circuit model as shown in Fig. 5*A* was proposed to represent the diffusion dialysis process using a CMM with ideal Li/Mg selectivity. Driven by the Donnan potentials ($\Delta\phi_+$ and $\Delta\phi_-$) across the membrane, the separate transport of Li^+ and Cl^- through the adjacent domains, together with the charge neutralization in the receiving solution, formed a local current loop (I_{loop}). The ionic flux (J) was directly proportional to the loop current density, which was in turn equal to the electromotive force (ξ) divided by the total areal resistance (R_{tot}):

$$J_{Cl} = J_{Li} = \frac{|I_{loop}|}{F} = \frac{|\xi|}{R_{tot}F}. \quad [1]$$

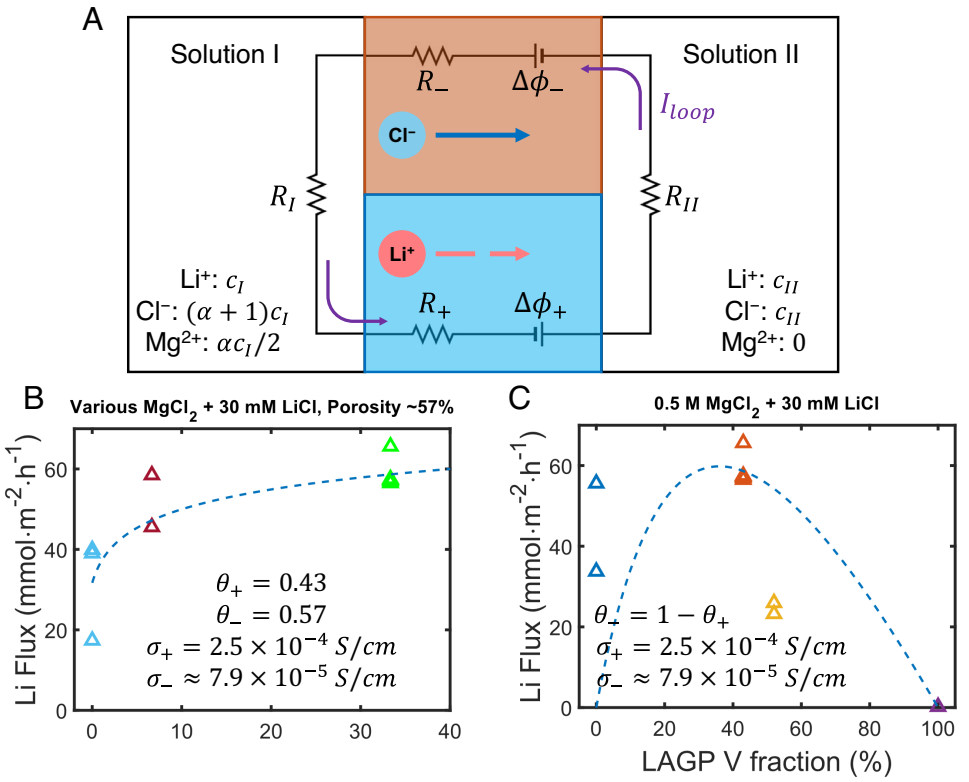

Fig. 5. Equivalent circuit model of the ion-sieving charge mosaic membrane. (*A*) Schematic illustration of the equivalent circuit model for Li/Mg separation through a charge mosaic membrane. The blue and orange blocks in the middle represent the lithium and anion conducting regions of the membrane respectively. The left and right blocks represent the adjacent feeding and receiving solution. Here both regions of the membrane are assumed to be ideal single ion conductors. (*B*) Fitted (dashed curve) versus experimental results of Li flux as a function of α, using the equivalent circuit model in the membrane-limited regime. The fitting parameter is the conductivity (σ_-) of the anion conducting region. (*C*) Model prediction versus experimental results of Li flux as a function of LAGP volume fraction in the membrane (θ_+). The prediction is made with the known and fitted parameters from *B*.

Here F is the Faraday constant. The total resistance was simply the sum of individual contributions from the anion and cation conductive membrane domains (R_- and R_+), as well as the nearby regions in the feeding and receiving solutions (R_I and R_{II}):

$$R_{tot} = R_+ + R_- + R_I + R_{II}. \quad [2]$$

At the beginning of diffusion dialysis tests, resistance of the receiving solution (R_{II}) should be the limiting factor because of the low salt concentration. However, the solution resistance quickly decreased, and the membrane resistance became dominating as the concentration (c_{II}) rose in the receiving solution. At a receiving concentration of 3 mM, the solution resistance was one order of magnitude smaller than the membrane resistance, as shown in *SI Appendix*, Note 2. When membrane resistance was limiting:

$$R_{tot} \approx R_+ + R_-,\ R_\pm = \frac{d}{\theta_\pm \sigma_\pm},\ \theta_- + \theta_+ = 1, \quad [3]$$

where d is the thickness of the membrane, $\theta_\pm$ represents the volume fraction of the Li and anion conductive domains, and $\sigma_\pm$ stands for their ionic conductivity respectively. Simplifying Eq. **3** gave the following expression for total resistance:

$$R_{tot} = \frac{\theta_+\sigma_+ + \theta_-\sigma_-}{\theta_+\sigma_+\theta_-\sigma_-} d. \quad [4]$$

On the other hand, the total electromotive force (ξ) could be calculated as the sum of the Donnan potentials $\Delta\phi_+$ and $\Delta\phi_-$, which were opposite in direction due to the selectivity towards oppositely charged ions:

$$|\xi| = \Delta\phi_+ + \Delta\phi_-. \quad [5]$$

The Donnan potentials $\Delta\phi_\pm$ developed as a result of the Gibbs–Donnan equilibrium, and their values could be derived from the concentration ratio of the corresponding ions across the membrane:

$$\Delta\phi_+ = \frac{RT}{F} ln(c_I/c_{II}), \quad [6]$$

$$\Delta\phi_- = \frac{RT}{F} ln((\alpha+1)c_I/c_{II}). \quad [7]$$

Here, R is the gas constant, T is the temperature, $\alpha + 1$ is the concentration ratio of Cl/Li ions, and c_I and c_{II} are the concentration of Li in the feeding and receiving solutions, respectively.

Substituting Eqs. **4**–**7** into Eq. **1**, we arrived at the final expression for the ionic flux across a CMM:

$$J = \frac{RT}{F^2 d} \frac{\theta(1-\theta)\sigma_+\sigma_-}{\theta\sigma_+ + (1-\theta)\sigma_-} \left[2ln\left(\frac{c_I}{c_{II}}\right) + ln(\alpha+1)\right]. \quad [8]$$

Here $\theta \equiv \theta_+$ is the volume fraction of LAGP. It is evident from Eq. **8** that the Li flux would scale with the logarithm of $\alpha + 1$, which is the Cl/Li concentration ratio. Therefore, the dependence of Li permeability on Cl concentration could be captured by our model.

By setting the derivative of J with respect to θ as zero, the optimal composition that maximizes the flux could be derived:

$$\theta_{opt} = \frac{1}{1 + \sqrt{\sigma_+/\sigma_-}}. \quad [9]$$

The model predicts that the more conductive phase should take a smaller volume fraction in an optimal membrane. This makes sense intuitively since the less conductive phase would need a larger volume fraction to minimize the total resistance. This optimal design strategy is easily generalizable because it only depends on the properties of the membrane materials.

To validate our model, we measured the ionic conductivity of pure LAGP membranes (*SI Appendix*, Fig. S13) to be 2.5×10^{-4} S · cm^{-1} and used this value to fit the experimental results. The model was able to fit the experimental data quite well in terms of the dependence of Li flux on α (Fig. 5*B*). The fitted value of pure AEP conductivity was 7.9×10^{-5} S · cm^{-1}, very close to the experimental results of 7.5×10^{-5} S · cm^{-1}. Using Eq. **8** and the fitted conductivity, the model also qualitatively reproduced the effect of composition observed in experiments (Fig. 5*C*). The deviation at $\theta = 0$ was likely a consequence of the nonideal anion selectivity of the AEP membrane. See *SI Appendix*, Note 2 for more details on the calculation of conductivity and the fitting process.

Discussion

In summary, this work reported on the design and construction strategies of charge mosaic membranes for sustainable Li extraction. Prepared by infiltrating an AEP into a porous LAGP pellet, the CMM featured bicontinuous conduction pathways selective to Li^+ and anions. Therefore, the membrane enabled high selectivity (~62) Li/Mg separation with high rate (59 mmol·m^{-2}·h^{-1}) and no external driving force. By adapting an equivalent circuit model, the coupled transport of Li^+ and anions through CMMs were described quantitatively. The dependence of transport rate (Li flux) on feeding brine compositions and membrane properties was systematically investigated in experiments, which successfully validated our model. Furthermore, the model also informed the optimal design that would maximize Li permeation rate, guiding the development of CMMs for other ion-sieving processes.

Compared to membranes with similar design reported in the literature (50, 59), our CMMs contained a larger fraction of anion exchange polymer. This enabled faster Li extraction with lower feeding concentration, but it also compromised the membrane selectivity due to the unsatisfactory anion selectivity of AEP. As a result, the Li/Na and Li/K selectivity of our high porosity CMM (57%) was only about 2 and 5, respectively (*SI Appendix*, Fig. S14). Similar to Li/Mg separation performance, CMM with lower porosity (48%) showed better Li/Na and Li/K selectivity but slower Li extraction rate. In order to further enhance the selectivity of CMMs, it is imperative to improve the quality of the AEP. Since commercial AEMs showed better anion selectivity than PECH-DABCO membranes we prepared (*SI Appendix*, Fig. S12), it is desirable to fabricate CMMs using these commercial materials. However, these membranes are very hard to dissolve, rendering the vacuum infiltration method inapplicable. Alternatively, embedding large LAGP particles into AEMs might be a better strategy, as demonstrated by Yang et al. (81), although suitable equipment and conditions need to be found. To increase Li flux, the easiest way would be to reduce the thickness of membrane, but this might compromise the selectivity. Instead, developing AEMs and Li-ion conductors with higher ionic conductivity will improve Li flux without sacrificing selectivity.

Expensive materials could be a major obstacle to scaling up membrane-based Li extraction techniques. In a preliminary techno-economic analysis (*SI Appendix*, Note 5), we have indeed noticed that the cost of LAGP precursor could be unaffordable. Fortunately, a low-cost and stable $Li_{1.5}Al_{0.3}Ti_{1.7}Si_{0.2}P_{2.8}O_{12}$ (LATSP) glass–ceramic electrolyte has been developed, which reduced the materials cost by a factor of 100 compared to LAGP(82). Utilizing this low-cost membrane material, the overall production cost of CMM-based extraction was estimated to be less than US$4,000 ton^{-1} (unit: US dollars per ton of lithium carbonate equivalent), very similar to the cost of redox-couple electrodialysis processes developed in our previous study (38). The analysis also highlighted the importance of membrane lifetime, which needs to be greater than roughly 3 mo for the processes to be profitable (*SI Appendix*, Table S4).

On the theoretical side, although the equivalent circuit model was effective in estimating the extraction rate, it did not take into account the influence of selectivity. Future models should study the impacts of individual selectivity of cation and anion channels on the overall selectivity of the CMMs. It would also be interesting to explore the effects of domain size, geometry, and external driving force on the ion-sieving performance of CMMs. As a preliminary step, we modified our model in Fig. 5 to include a cation leakage resistance to the anion conducting branch (*SI Appendix*, Fig. S15), representing the nonideal selectivity of AEP. The detailed derivation is shown in *SI Appendix*, Note S4. The leakage current I_{leak} is shown to be proportional to $1 - t_-$, where t_- is the anion transference number of the AEP. The generalized model could also predict the instantaneous Li selectivity of CMM, which establishes a more realistic theoretical framework for future studies.

Materials and Methods

Preparation of Porous LAGP Membrane. LAGP powder was purchased from MSE Supplies LLC. The LAGP powder was mixed with cellulose in a ratio of 2:1 or 1:1 and ground uniformly. The mixed powder (0.3 g) was pressed in a die set under constant uniaxial pressure of 20 MPa for 1 min. The pressed pellet was then sintered at 500 °C for 2 h and 850 °C for 4 h in a tube furnace. The sintered porous LAGP pellets had a diameter of about 16.0 mm. Dense LAGP pellets were pressed with 0.3 g pure LAGP powder and sintered at 850 °C for 6 h in a tube furnace.

Preparation of PECH-DABCO and the Composite Membrane. PECH was purchased from Scientific Polymer Products Inc. DABCO was purchased from MilliporeSigma. DMSO was purchased from MilliporeSigma. First, 0.5 g of PECH was dissolved in 7.5 mL of DMSO at 60 °C, followed by the addition of 5 mL of DABCO solution (0.6 g of DABCO dissolved in 5 mL of DMSO). The mixture was then stirred at 70 °C overnight to obtain PECH-DABCO. The PECH-DABCO solution was then dropped onto the porous LAGP membrane and placed in a vacuum oven at 60 °C to perform vacuum infiltration overnight. Afterward, the composite membrane was placed into DI water to get rid of the extra AEP on its surface. The membrane was then attached onto a circular hole in an acrylic panel using epoxy glue. The exposed area of LAGP was designed as 1 cm^2.

Material Characterization. Fourier transform infrared (FT-IR, Nicolet iS50) spectroscopy was used to characterize the synthesized PECH-DABCO polymer in comparison with the PECH polymer and DABCO crystal before crosslinking. X-ray photoelectron spectroscopy (XPS, PHI VersaProbe III with a monochromatized Al(Kα) X-ray Source) was used to characterize the formation of quaternary ammonium groups. The crystalline structure of LAGP membranes was analyzed by X-ray diffraction (XRD, PANalytical Empyrean with a Cu(Kα) X-ray source). Diffraction patterns were collected from 10° to 70° using a step size of 0.01°. A scanning

electron microscope (SEM, Thermo Fisher Scientific Apreo) was used to investigate the microstructural evolution of porous LAGP and composite membrane. Nitrogen gas adsorption experiments were conducted on Anton Paar Autosorb iQ3 particle analyzer to study the pore volume and size distribution.

Diffusion Dialysis Tests for Li Extraction. The H-shaped electrochemical cell was purchased from Adams and Chittenden Scientific Glass. The composite membrane attached on the acrylic panel, prepared with different porosities, was sandwiched between the two chambers of an H-cell and sealed with two rubber O-rings and a clamp. The two chambers each contained 50 mL of solution and were continuously stirred with a magnetic stirrer. The feeding solution was 30 mM LiCl with various concentrations of $MgCl_2$ as indicated in the main text, unless mentioned otherwise. The receiving solution was deionized water unless mentioned otherwise. At intervals of 1, 2, 4, 8, 16, 24, 48, and 72 h, 50 μL of the feeding solution and receiving solution were collected and then diluted with a 2% aqueous nitric acid solution for Inductively Coupled Plasma Mass Spectrometry (ICP-MS) analysis (Thermo Scientific XSERIES 2 Quadrupole).

The impedance of the cell was determined by the electrochemical impedance spectroscopy (EIS) (Biologic VMP3 system) with a frequency range from 1 MHz to 0.1 Hz and a perturbation voltage of 10 mV at room temperature.

Calculation of the Faradaic Efficiency, Li Selectivity, and Energy Output. The extraction rate was calculated by

$$r = \frac{V\Delta C_{Li^+}}{A \cdot t},$$

where $V(L)$ is the volume of the receiving solution in the cell, $\Delta C_{Li^+}(mmol \cdot L^{-1})$ is the variation of Li ion concentration in the receiving solution, $A(m^2)$ is the area of the membrane, and $t(h)$ is the testing duration. The Li/Mg selectivity factor was calculated by

$$S = \frac{\Delta C_{Li^+} \cdot C_{Mg^{2+},0}}{\Delta C_{Mg^{2+}} \cdot C_{Li^+,0}},$$

where $\Delta C_{Mg^{2+}}$ is the variation of Mg-ion concentration in the receiving solution, $C_{Mg^{2+},0}$ and $C_{Li^+,0}$ are the initial concentration of Mg and Li in the feeding solution.

Data, Materials, and Software Availability. All study data are included in the article and/or *SI Appendix*.

ACKNOWLEDGMENTS. This work was supported by the Stanford StorageX Initiative. Part of this work was performed at the Stanford Nano Shared Facilities, supported by the NSF under Award ECCS-2026822. Part of this work was performed in the nano@Stanford labs, supported by the NSF as part of the National Nanotechnology Coordinated Infrastructure under Award ECCS-1542152.

Author affiliations: [a]Department of Materials Science and Engineering, Stanford University, Stanford, CA 94305; [b]Stanford Institute for Materials and Energy Sciences, SLAC National Accelerator Laboratory, Menlo Park, CA 94025; and [c]Department of Energy Science and Engineering, Stanford University, Stanford, CA 94305

1. P. Greim, A. A. Solomon, C. Breyer, Assessment of lithium criticality in the global energy transition and addressing policy gaps in transportation. *Nat. Commun.* **11**, 4570 (2020).
2. B. E. Lebrouhi *et al.*, Key challenges for a large-scale development of battery electric vehicles: A comprehensive review. *J. Energy Storage* **44**, 103273 (2021).
3. Y. M. Huang, J. Li, Key challenges for grid-scale lithium-ion battery energy storage. *Adv. Energy Mater.* **12**, 2202197 (2022).
4. G. Martin, L. Rentsch, M. Höck, M. Bertau, Lithium market research–Global supply, future demand and price development. *Energy Storage Mater.* **6**, 171–179 (2017).
5. A. Kumar, H. Fukuda, T. A. Hatton, J. H. V. Lienhard, Lithium recovery from oil and gas produced water: A need for a growing energy industry. *ACS Energy Lett.* **4**, 1471–1474 (2019).
6. C. B. Tabelin *et al.*, Towards a low-carbon society: A review of lithium resource availability, challenges and innovations in mining, extraction and recycling, and future perspectives. *Miner. Eng.* **163**, 106743 (2021).
7. O. A. Kazi *et al.*, Material design strategies for recovery of critical resources from water. *Adv. Mater.* **35**, 2300913 (2023).
8. F. Degen, M. Winter, D. Bendig, J. Tübke, Energy consumption of current and future production of lithium-ion and post lithium-ion battery cells. *Nat. Energy* **8**, 1284–1295 (2023).
9. A. Mas-Fons *et al.*, Carbon and water footprint of battery-grade lithium from brine and spodumene: A simulation-based LCA. *J. Clean. Prod.* **452**, 142108 (2024).
10. W. F. D. Paz *et al.*, The water footprint of lithium extraction technologies: Insights from environmental impact reports in Argentina's salt flats. *Heliyon* **11**, e42523 (2025).
11. M. L. Vera, W. R. Torres, C. I. Galli, A. Chagnes, V. Flexer, Environmental impact of direct lithium extraction from brines. *Nat. Rev. Earth Environ.* **4**, 149–165 (2023).
12. C. Violet *et al.*, Designing membranes with specific binding sites for selective ion separations. *Nat. Water* **2**, 706–718 (2024).
13. J. D. Ying, Y. Q. Lin, Y. R. Zhang, J. G. Yu, Developmental progress of electrodialysis technologies and membrane materials for extraction of lithium from salt lake brines. *ACS ES&T Water* **3**, 1720–1739 (2023).
14. X. P. Tian *et al.*, Enhancing membrane materials for efficient Li recycling and recovery. *Adv. Mater.* **37**, 2402335 (2025).
15. J. Hou *et al.*, Lithium extraction by emerging metal-organic framework-based membranes. *Adv. Funct. Mater.* **31**, 2105991 (2021).
16. H. Wen, Z. Y. Liu, J. J. Xu, J. P. Chen, Nanofiltration membrane for enhancement in lithium recovery from salt-lake brine: A review. *Desalination* **591**, 117967 (2024).
17. L. Zhang *et al.*, A review of the nanofiltration membrane for magnesium and lithium separation from salt-lake brine. *Sep. Purif. Technol.* **354**, 129169 (2025).
18. B. Tansel *et al.*, Significance of hydrated radius and hydration shells on ionic permeability during nanofiltration in dead end and cross flow modes. *Sep. Purif. Technol.* **51**, 40–47 (2006).
19. A. Razmjou, M. Asadnia, E. Hosseini, A. Habibnejad Korayem, V. Chen, Design principles of ion selective nanostructured membranes for the extraction of lithium ions. *Nat. Commun.* **10**, 5793 (2019).
20. J. Q. Luo, Y. H. Wan, Mix-charged nanofiltration membrane: Engineering charge spatial distribution for highly selective separation. *Chem. Eng. J.* **464**, 142689 (2023).
21. B. B. Guo *et al.*, Double charge flips of polyamide membrane by ionic liquid-decoupled bulk and interfacial diffusion for on-demand nanofiltration. *Nat. Commun.* **15**, 2282 (2024).
22. H. Z. Zhang, Z. L. Xu, H. Ding, Y. J. Tang, Positively charged capillary nanofiltration membrane with high rejection for $Mg^{2+}$and Ca^{2+} and good separation for Mg^{2+} and Li^+. *Desalination* **420**, 158–166 (2017).
23. W. Li *et al.*, A positively charged composite nanofiltration membrane modified by EDTA for LiCl/$MgCl_2$ separation. *Sep. Purif. Technol.* **186**, 233–242 (2017).
24. Y. N. Liu *et al.*, Pillared laminar vermiculite membranes with tunable monovalent and multivalent ion selectivity. *Adv. Mater.* **37**, 2417994 (2025).
25. T. Ye *et al.*, Highly selective lithium transport through crown ether pillared angstrom channels. *Angew. Chem. Int. Ed.* **63**, e202316161 (2024).
26. R. Tan *et al.*, Hydrophilic microporous membranes for selective ion separation and flow-battery energy storage. *Nat. Mater.* **19**, 195–202 (2020).
27. J. Lu *et al.*, Efficient metal ion sieving in rectifying subnanochannels enabled by metal-organic frameworks. *Nat. Mater.* **19**, 767–774 (2020).
28. S. Kunugi, Y. Inaguma, M. Itoh, Electrochemical recovery and isotope separation of lithium ion employing lithium ion conductive perovskite-type oxides. *Solid State Ion.* **122**, 35–39 (1999).
29. T. Hoshino, Innovative lithium recovery technique from seawater by using world-first dialysis with a lithium ionic superconductor. *Desalination* **359**, 59–63 (2015).
30. Z. Li *et al.*, Continuous electrical pumping membrane process for seawater lithium mining. *Energy Environ. Sci.* **14**, 3152–3159 (2021).
31. F. Y. Fan *et al.*, A bioinspired membrane with ultrahigh Li^+/Na^+ and Li^+/K^+ separations enables direct lithium extraction from brine. *Adv. Sci.* **11**, 2402898 (2024).
32. S. K. Patel, A. Iddya, W. Y. Pan, J. H. Qian, M. Elimelech, Approaching infinite selectivity in membrane-based aqueous lithium extraction via solid-state ion transport. *Sci. Adv.* **11**, eadq9823 (2025).
33. K. Sasaki, R. Hiraka, H. Takahashi, K. Shin-mura, Energy balance of lithium recovery by electrodialysis using La0.57Li0.29TiO3 electrolyte. *Fusion Eng. Des.* **170**, 112500 (2021).
34. H. Huang *et al.*, Photoelectrochemical lithium extraction. *Nano Energy* **115**, 108683 (2023).
35. Z. Li *et al.*, Green lithium: Photoelectrochemical extraction. *PhotoniX* **4**, 23 (2023).
36. L. Wang *et al.*, Redox flow battery for continuous and energy-effective lithium recovery from aqueous solution. *ACS Energy Lett.* **7**, 3539–3544 (2022).
37. R. X. Xie *et al.*, Ecofriendly, highly selective lithium extraction by redox-mediated electrodialysis. *ACS Central Sci.* **10**, 2119–2124 (2024).
38. R. Xu *et al.*, Continuous lithium extraction from brine by efficient redox-couple electrodialysis. *Matter* **7**, 3876–3890 (2024).
39. G. Zhang *et al.*, Spontaneous lithium extraction and enrichment from brine with net energy output driven by counter-ion gradients. *Nat. Water* **2**, 1091–1101 (2024).
40. J. N. Weinstein, S. R. Caplan, Charge-mosaic membranes–Enhanced permeability and negative osmosis with a symmetrical salt. *Science* **161**, 70–72 (1968).
41. K. Söllner, On mosaic membranes. *Biochem. Z* **244**, 370–381 (1932).
42. R. Neihof, K. Sollner, A quantitative electrochemical theory of the electrolyte permeability of mosaic membranes composed of selectively anion-permeable and selectively cation-permeable parts and its experimental verification. 1. An outline of the theory and its quantitative test in model systems with auxiliary electrodes. *J. Phys. Colloid. Chem.* **54**, 157–176 (1950).
43. R. Neihof, K. Sollner, A quantitative electrochemical theory of the electrolyte permeability of mosaic membranes composed of selectively anion-permeable and selectively cation-permeable parts, and its experimental verification. 2. A quantitative test of the theory in model systems which do not involve the use of auxiliary electrodes. *J. Gen. Physiol.* **38**, 613–622 (1955).
44. S. Rajesh, Y. Yan, H. C. Chang, H. F. Gao, W. A. Phillip, Mixed mosaic membranes prepared by layer-by-layer assembly for ionic separations. *ACS Nano* **8**, 12338–12345 (2014).
45. F. Gao *et al.*, Interfacial junctions control electrolyte transport through charge-patterned membranes. *ACS Nano* **13**, 7655–7664 (2019).
46. M. Higa *et al.*, Preparation of PVA-based charged mosaic membrane using screen-printed method and evaluation of ion transport properties. *J. Membr. Sci.* **711**, 123158 (2024).
47. T. Ounissi *et al.*, Novel lithium selective composite membranes: Synthesis, characterization and validation tests in dialysis. *J. Mater. Sci.* **55**, 16111–16128 (2020).

48. T. Ounissi, L. Dammak, J. F. Fauvarque, E. Selmane Bel Hadj Hmida, Ecofriendly lithium-sodium separation by diffusion processes using lithium composite membrane. *Sep. Purif. Technol.* **275**, 119134. (2021).
49. T. Ounissi *et al.*, Lithium-sodium separation by a lithium composite membrane used in electrodialysis process: Concept validation. *Membranes* **12**, 244 (2022).
50. H. Y. Ma *et al.*, Dual-channel-ion conductor membrane for low-energy lithium extraction. *Environ. Sci. Technol.* **57**, 17246–17255 (2023).
51. R. Q. Zheng *et al.*, Enhancing ion selectivity of nanofiltration membranes via heterogeneous charge distribution. *Environ. Sci. Technol.* **58**, 22818–22828 (2024).
52. V. I. Kovalenko, A. A. Akhmadiyarov, A. E. Vandyukov, A. R. Khamatgalimov, Experimental vibrational spectra and computational study of 1, 4-diazabicyclo[2.2.2]octane. *J. Mol. Struct.* **1028**, 134–140 (2012).
53. X. J. Zeng *et al*., Anionic MOFs embedded in anion-exchange membranes for the separation of lithium/magnesium cations. *ACS Sustain. Chem. Eng.* **11**, 12877–12887 (2023).
54. U. Habiba *et al.*, Porous alumina-supported lithium aluminum titanium phosphate membrane for lithium extraction using the electrodialysis process. *Sep. Purif. Technol.* **354**, 128657 (2025).
55. L. P. Guo, Z. Y. Guo, J. Wang, Z. H. Huang, Z. Y. Ji, Flexible lithium selective composite membrane for direct lithium extraction from high Na/Li ratio brine. *J. Membr. Sci.* **703**, 122843 (2024).
56. J. S. Chen *et al.*, Electronanofiltration membranes with a bilayer charged structure enable high Li/Mg selectivity. *ACS Appl. Mater. Inter.* **16**, 6632–6643 (2024).
57. X. Ruan *et al.*, Constructing mechanical shuttles in a three-dimensional (3D) porous architecture for selective transport of lithium ions. *Angew. Chem. Int. Ed.* **62**, e202216549 (2023).
58. H. M. Saif, R. M. Huertas, S. Pawlowski, J. G. Crespo, S. Velizarov, Development of highly selective composite polymeric membranes for Li^+/Mg^{2+} separation. *J. Membr. Sci.* **620**, 118891 (2021).
59. D. Seo, J. Lee, S. R. Kong, G. Sim, Y. Park, Selective lithium extraction from salt-lake brine using LATP-incorporated cellulose membranes in electrically driven systems. *J. Membr. Sci.* **718**, 123676 (2025).
60. H. Peng *et al.*, Quaternization-spiro design of chlorine-resistant and high-permeance lithium separation membranes. *Nat. Commun.* **14**, 5483 (2023).
61. Y. Zhang, Z. Hao, I. Hussein, Z. Wang, S. Zhao, Tunable ionic sieving membrane via reactive layer-by-layer assembly of porous organic cages. *Adv. Funct. Mater.* **34**, 2315750 (2024).
62. M. Yong *et al.*, Sustainable lithium extraction and magnesium hydroxide co-production from salt-lake brines. *Nat. Sustain.* **7**, 1662–1671 (2024).
63. H. W. Peng, Q. Zhao, A nano-heterogeneous membrane for efficient separation of lithium from high magnesium/lithium ratio brine. *Adv. Funct. Mater.* **31**, 2009430 (2021).
64. G. J. Zhao, H. Q. Gao, Z. Qu, H. W. Fan, H. Meng, Anhydrous interfacial polymerization of sub-1 Å sieving polyamide membrane. *Nat. Commun.* **14**, 7624 (2023).
65. S. S. Hong *et al.*, Precision ion separation via self-assembled channels. *Nat. Commun.* **15**, 3160 (2024).
66. H. Peng, X. Liu, Y. Su, J. Li, Q. Zhao, Advanced lithium extraction membranes derived from tagged-modification of polyamide networks. *Angew. Chem. Int. Ed.* **62**, e202312795 (2023).
67. Z. Lu, Y. Wu, L. Ding, Y. Wei, H. Wang, A Lamellar MXene ($Ti_3C_2T_x$)/PSS composite membrane for fast and selective lithium-ion separation. *Angew. Chem. Int. Ed.* **60**, 22265–22269 (2021).
68. J. Zhao, R. Y. Fan, S. C. Xiang, J. P. Hu, X. M. Zheng, Preparation and lithium-ion separation property of ZIF-8 membrane with excellent flexibility. *Membranes* **13**, 500 (2023).
69. Y. Dong *et al.*, Crown ether-based Troger's base membranes for efficient Li^+/Mg^{2+}separation. *J. Membr. Sci.* **665**, 121113 (2023).
70. S. S. Bing *et al.*, Bio-inspired construction of ion conductive pathway in covalent organic framework membranes for efficient lithium extraction. *Matter* **4**, 2027–2038 (2021).
71. L. Fu *et al.*, Construction of a hierarchical membrane with angstrom-scale ion channels for enhanced Li^+/Mg^{2+}separation. *Chem. Commun.* **59**, 9384–9387 (2023).
72. C. Zhang, Y. Mu, W. Zhang, S. Zhao, Y. Wang, PVC-based hybrid membranes containing metal-organic frameworks for Li^+/Mg^{2+} separation. *J. Membr. Sci.* **596**, 117724 (2020).
73. G. Z. Luo *et al.*, Lithium-ion-sieve-embedded hybrid membranes for anion-exchange- and cation-concentration-driven Li/Mg separation. *ACS Appl. Mater. Inter.* **16**, 66911–66920 (2024).
74. Y. Y. Zhang *et al.*, Congener-welded crystalline carbon nitride membrane for robust and highly selective Li/Mg separation. *Sci. Adv.* **10**, eadm9620 (2024).
75. T. Wu *et al.*, Imine-linked 3D covalent organic framework membrane featuring highly charged Sub-1 nm channels for exceptional lithium-ion sieving. *Adv. Mater.* **37**, 2415509 (2025).
76. Y. S. Hou *et al.*, Artificial cation-chloride co-transporters for chloride-facilitated lithium/magnesium separation. *Angew. Chem. Int. Ed.* **64**, e202504259 (2025).
77. J. N. Weinstein, B. J. Bunow, S. R. Caplan, Transport properties of charge-mosaic membranes. 1. Theoretical models. *Desalination* **11**, 341–377 (1972).
78. J. N. Weinstein, B. M. Misra, D. Kalif, S. R. Caplan, Transport properties of charge-mosaic membranes. 2. Experimental studies. *Desalination* **12**, 1–17 (1973).
79. A. E. Yaroshchuk, An analytical solution for the diffusion of electrolytes through a charge-mosaic membrane. *Phys. Chem. Chem. Phys.* **3**, 1883–1890 (2001).
80. M. J. Summe, S. J. Sahoo, J. K. Whitmer, W. A. Phillip, Salt permeation mechanisms in charge-patterned mosaic membranes. *Mol. Syst. Des. Eng.* **3**, 959–969 (2018).
81. J. G. Yang *et al.*, Lithium metal recovery from sea water by a flexible and scalable membrane with lithium-ion exclusive channels. *Angew. Chem. Int. Ed.* **63**, e202411957 (2024).
82. B. Chang *et al.*, Low-cost and stable $Li_{1.5}Al_{0.3}Ti_{1.7}Si_{0.2}P_{2.8}O_{12}$ glass–ceramics for lithium extraction from seawater. *J. Solid State Electrochem.* **28**, 4131–4139 (2024).